Continuous High-Resolution Earth Observation with Multiple Aperture Optical Telescopes.

L. Mugnier, F. Cassaing, G. Rousset, F. Baron, V. Michau, I. Mocœur, B. Sorrente and M.-T. Velluet. *

OPTRO 2005.

Abstract

ONERA has recently completed a study on the feasibility of an imaging interferometer for Earth observation from a GEO orbit. During this study, some key elements for the definition of such an instrument have been identified and studied. They include the optical design, the cophasing of the instrument on a wide field, the aperture configuration (*i.e.*, the relative positioning of the individual telescopes that interfere together), and the restoration of the recorded images. The cophasing has been validated experimentally. The results obtained confirm the applicability of wide-field optical interferometry with a Michelson-type instrument for Earth observation from a GEO orbit.

Keywords : Earth observation; interferometry; synthetic aperture optics; multiple apterture telescope; optical design; cophasing sensor; aperture configuration optimization; image restoration.

1 Introduction

The permanent and high-resolution monitoring of Earth would be a breakthrough with numerous, civilian and defense, applications. Permanence goes hand in hand with the use of a high-altitude orbit and thus an increase of the angular resolution of the imaging instrument with respect to that of a low earth orbit satellite, for the same on-ground resolution.

ONERA has recently completed a study on the feasibility of an imaging interferometer, also called Multiple Aperture Optical Telescope (MAOT), for high-resolution Earth observation from a geostationary (GEO) orbit. During this study, some key elements for the definition of such an instrument have been identified and studied. They include the optical design, the cophasing of the instrument on a wide field, the aperture configuration (*i.e.*, the relative positioning of the individual telescopes that interfere together), and the restoration of the recorded images. The cophasing has been validated experimentally.

Sections 2 to 5 review the results obtained on these key issues. In the rest of this contribution, we assume that the images of the instrument will have a pixel size of 1 m and will be Nyquist-sampled at a wavelength of $\lambda = 0.5\mu$m. For a GEO orbit, this leads to a "baseline" (diameter of an equivalent monolithic telescope) $B \approx 10$ m.

2 Optical design of a Michelson-type Multiple Aperture Optical Telescope

Two families of optical designs can be considered for a MAOT [1]:

*ONERA/DOTA/CC, BP 72, 92322 Châtillon cedex, France.

- the “Fizeau” design (Fig. 1a): the aperture segments are portions of a common primary mirror. The length L is close to the maximum baseline B;
- the “Michelson” design (Fig. 1b): independent telescopes are combined by a dedicated telescope. The length L is close to the telescope diameter D.

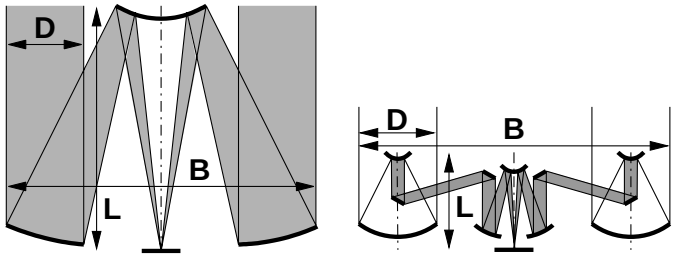

(a) (b)

Figure 1: Principle of Fizeau (a) and Michelson (b) MAOTs, with the same maximum baseline B and sub-aperture diameter D.

Famous Fizeau designs are each Keck Telescope or the JWST. The Michelson design is mainly used by ground-based stellar interferometers, such as the VLT-I or the Keck-I, with very diluted aperture and a very small field. But direct wide-field focal-plane imaging with a Michelson MAOT, as illustrated in Fig. 1b, is also possible provided some optical conditions such as homothetic pupil mapping [2] are met. It has been experimentally pioneered by the Multi-Mirror Telescope (MMT) [3], the Multi-Mirror Telescope Tested (MMTT) [4], the Multi-ap [5]. Very wide field imaging has been validated by simulation with complex designs [6, 7].

The choice between the Michelson and Fizeau designs is a complex system task involving optical design and manufacturing, mechanical design, etc. Such a trade-off that can only be performed once the detailed performance of each design is known. Fizeau MAOTs can be considered as masked monolithic telescopes, so they can be simply designed, optimized and characterized with classical optical-design softwares. But to the best of our knowledge, no optical-design software can perform optimization with parallel propagation in several arms. Therefore, the design of a Michelson MAOT is a sophisticated task, which relies heavily on the designer’s physical intuition and know-how. Indeed, many specific constraints must be considered simultaneously, as investigated and progressively understood by many authors for astronomy or wide-field imaging [2, 8, 6, 9, 10, 11].

We investigated in details the design and optimization of a Michelson MAOT. To this aim, we have developed a computer tool, based on the analytical computation of the aberrations in the sub-telescopes and periscopes of Michelson MAOTs. Such an analytical approach gives more physical insight for each free design parameter and allows one to better control the optimization.

The main result of this study is that a very wide field can be obtained with rather simple designs based on 2-mirror sub-telescopes, mainly by using a small D/B ratio [12]. Most other authors propose more complex designs based on at least 3-mirror sub-telescopes. For example, Fig. 2 shows the configuration we used to validate our analytical study by an independent Zemax computation. It is made of 4 Mersenne sub-telescopes (two confocal paraboloids) combined with a classical 3-mirror Korsch telescope. The linear configuration can be extrapolated to a 2D configuration with same

performance, using more telescopes, as described in section 4. The Strehl ratio estimated from the wavefront error originating from optical design is larger than 0.95 over a field of 15 000 resolution elements.

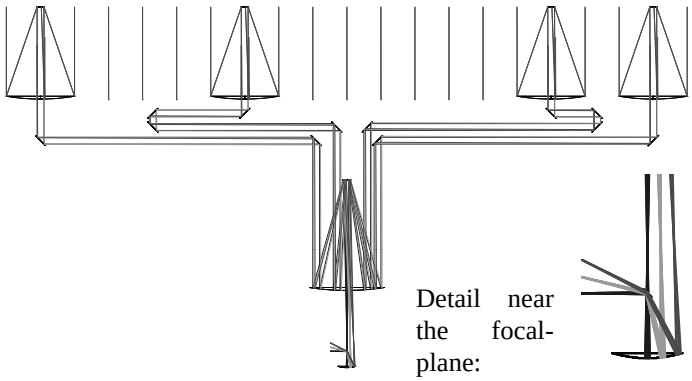

Figure 2: Optical design of a diffraction limited MAOT with a maximum baseline B=10 m and sub-telescopes with diameter D=1 m.

3 Cophasing on a wide field

3.1 Selection of a cophasing sensor

For correct performance, the aperture of an imaging instrument must be phased to a small fraction of the wavelength. For a 10 m aperture diameter in the visible as considered here, this leads to a figure control better than 1 part in 10^8 which can most likely not be met passively. A critical sub-system of interferometers is thus the cophasing sensor (CS), whose goal is to measure the relative positioning (differential piston and tip/tilt) of the sub-apertures, which are the main sources of wave-front degradations, and possibly the higher-order aberrations on each sub-aperture. Even if the instrument can be stabilized by a complex internal metrology, we believe that an external sensor, based on the analysis of the observed scene, is required to cancel drifts induced by differential paths [13, 1].

Measurement of tip/tilt or of higher-order aberration modes by wave-front sensors is now a well established technique for monolithic telescopes, even on very extended objects such as the Earth seen from space [14]. Piston measurement has also been widely studied for metrology sensors, and piston compensation of distant telescopes has been demonstrated with non cooperative sources on the ground [15, 16]. But for most of these devices based on a pupil-plane combination, the contrast of interference fringes strongly decreases as the extension of the observed scene (or object) increases, which makes them useless on very extended scenes. To overcome this problem, specific kinds of fringe sensors have been proposed.

A first solution is spatial filtering (SF) with a field stop in each sub-telescope, to extract a spot from the scene [17]. The main drawback of this technique proposed for Sun observation is that since the field stop dimension must be close to the sub-aperture resolution, only a very small amount of the scene flux is used, which is not acceptable for Earth observation. In addition, to ensure a high fringe visibility, a high pointing accuracy must be achieved on each telescope and the ratio D/B must be kept small.

Table 1: Summarized comparison between spatial filtering and phase diversity for cophasing.

Criterion	Spatial Filtering	Phase Diversity
Optical setup	complex	**simple**
$\gg$2 beams	complex	**simple**
Flux	huge loss	**no loss**
Tip/tilt compensation	required	**not required**
Tip/tilt measurement	no	**yes**
Higher order modes meas^{t}.	no	**yes**
Data processing	**simple**	complex

Another solution is phase diversity (PD), a focal-plane technique based on the observation of at least two images of the same object to simultaneously solve for the unknown object and phase. While originally introduced for monolithic telescopes [19], PD has been extended to MAOTs [20] and has been experimentally validated on a MAOT laboratory breadboard [21]. We have shown that when used for phase measurement, the object can be integrated out of the problem and that this "marginal" PD is more efficient on monolithic telescopes than the classical joint PD methods [22, 23]. Simulations show that marginal PD is also a good solution for MAOT cophasing [24]. An important feature of PD is that complexity is reported on the software: a simple optical hardware theoretically allows the simultaneous measurement of many Zernike modes on a large number of sub-apertures.

The comparison between these two solutions is summarized in Table 1. Other investigated solutions, such as Hartmann-Shack wavefront sensors with sub-apertures overlapping adjacent MAOT sub-pupils [25], are not suited for large sub-telescope spacing and are not reported here. PD is based on the analysis of the image produced naturally by the MAOT, whereas SF requires a dedicated optical device (inducing differential paths) to insert field stops and implement the pairwise pupil-plane combination, which allows a simple phase computation. A multiple-beam focal-plane combination can also be used with SP, but the data processing is then quite similar to that of PD.

The best solution for Earth observation, according to Table 1, is phase diversity. To test its performance, a prototype sensor and a laboratory bench have been built.

3.2 Experimental results

We have designed, built and validated a prototype phase diversity CS for Earth observation. After a short presentation of this prototype and its testbed, we present its latest results. A more comprehensive presentation of the testbed along with earlier results can be found in [18, 26].

A schematic view of the testbed, called BRISE for Banc Reconfigurable d'Imagerie sur Scènes Etendues, is shown on Fig. 3. BRISE is mainly composed of four modules (source, perturbation, detection and control), described below.

The source module delivers two objects: an extended scene, which is an Earth scene on a high-resolution photographic plate illuminated by an arc-lamp, and a reference point source, which is the output of a monomode fiber fed with a He-Ne laser.

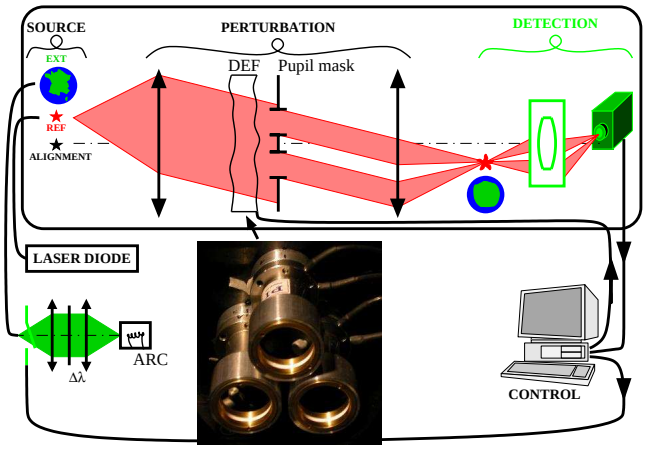

Figure 3: Schematic view of the BRISE testbed and photograph of the deformable mirror (DEF).

The perturbation module has three functions: it images the source on the detector, defines the aperture configuration and introduces calibrated aberrations; its main component is the deformable mirror (DM), which performs the latter function. In order to introduce only piston and tip/tilt, we have chosen to manufacture a specific segmented DM consisting of three planar mirrors mounted on piezo-actuated platforms by Physik Instrument, which have exactly these three degrees of freedom.

The detection module is a water-cooled CCD camera that simultaneously records a focal-plane image and a defocused image of each of the two objects to implement a phase diversity CS. Figure 4 shows an experimental example of such an image. The control module drives the experiment.

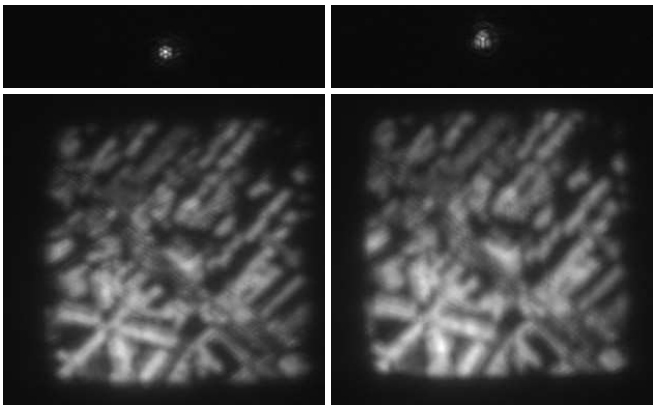

Figure 4: Focused (left) and defocused (right) experimental images of the extended scene (bottom) and reference point source (top) objects. These images are recorded simultaneously on different parts of the same detector and used for phase diversity.

Special care has been given to the control of errors that could limit CS performance

or the evaluation of the CS performance on extended objects. In particular, the two objects are observed simultaneously through very close paths, to minimize the differential effects of field aberrations, vibrations or air turbulence. A very accurate aberration calibration can thus be achieved thanks to the high SNR of the measurement obtained on the reference point source.

Figure 5 presents the piston measured at high photon level on a given sub-aperture as a function of the piston effectively introduced by the DM, for the reference point source at $\lambda_r = 633\,\text{nm}$ and for the extended scene, illuminated with white light and a spectral filter of width $40\,\text{nm}$ centered around $\lambda_e = 650\,\text{nm}$. For each introduced piston, three measurements are performed and reported on this figure. The point-source measurements exhibit an excellent linearity between roughly $-\lambda_r/2$ and $+\lambda_r/2$, at which points the expected modulo 2π wrapping occurs. With the extended object, the curve is linear on a slightly smaller piston range. Some features are different on this curve with respect to the one obtained with the reference point: the slope is not exactly unity, although this would not be a major problem in closed loop, and the sort of smooth wraparound that occurs around $+\lambda_e/2$ is somewhat surprising and currently interpreted as a consequence of the spectral bandwidth. Figure 6 shows the repeatability obtained

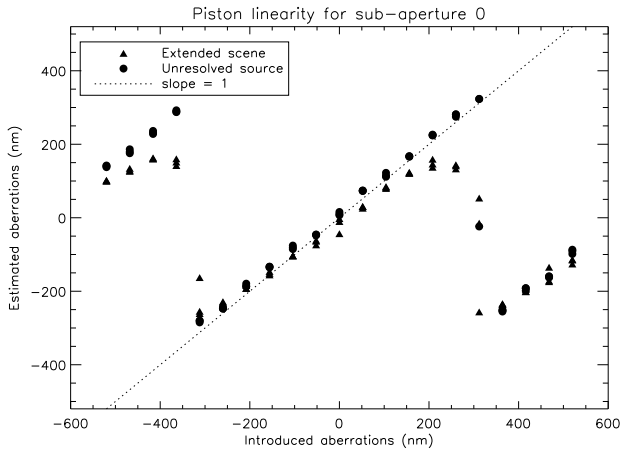

Figure 5: Piston measured at high photon level on the first sub-aperture, as a function of the piston effectively introduced by the DM.

on the piston measurement with the extended object. The standard deviation of the estimated piston is, as expected, dominated by detector noise for low fluxes, and then inversely proportional to the square root of the number of photons per pixel (photon-noise regime). It is for instance below $1\,\text{nm}$ as soon as the average flux is above 1000 photo-electrons per pixel.

4 Aperture configuration optimization

4.1 Introduction

The relative arrangement of the elementary telescopes (the so-called aperture configuration, or pupil configuration) is a key aspect of the design of a interferometer. There

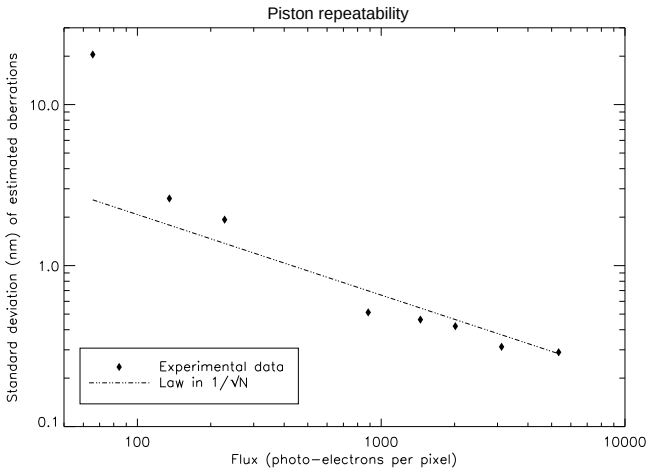

Figure 6: Repeatability obtained on the measurement of the piston on the first subaperture with the extended object, as a function of the average photon level per pixel.

is an abundant literature on this subject in radio astronomy. More recently, many papers have discussed this subject with respect to optical instruments (see, e.g., [27] for a review and extensive references). Here, we focus on imaging MAOTs, which form images of the observed object in a focal plane, as opposed to optical interferometers such as the VLTI, which provide only visibilities (Fourier samples of the observed object).

The purpose of the following is to derive a criterion for aperture configuration optimization of imaging MAOTs under constraints such as the total collecting surface and the system complexity (e.g., the number of apertures or their sizes).

4.2 Optimality criterion for aperture configuration

We consider an imaging MAOT whose field aberrations can be neglected. The recording process is modeled as:

$$\boldsymbol{i} = \boldsymbol{h} \star \boldsymbol{o} + \boldsymbol{n} \tag{1}$$

where $\boldsymbol{o}$ is the observed object (scene), $\boldsymbol{i}$ is the recorded image, $\boldsymbol{n}$ is an additive noise and $\star$ denotes a convolution.

As mentioned in the introduction, the quantity of utmost interest is not the raw image, but rather the object that can be estimated from this image. Here, we choose to perform the restoration by means of the Wiener filter, because it is optimal in the mean-square sense in the class of linear filters and because it lends itself to analytical calculations. The estimated object is then, in Fourier space:

$$\tilde{o}_e = \frac{\tilde{i}\,\tilde{h}^*}{|\tilde{h}|^2 + S_n/S_o} \tag{2}$$

where $\tilde{\cdot}$ denotes Fourier transformation and S_n and S_o are the power spectral densities (PSD) of the noise and of the object respectively.

The restoration error ϵ can be defined as the RMS difference between the original object $\boldsymbol{o}$ and its estimate $\boldsymbol{o}_e$: $\epsilon^2 \triangleq \sum_{k,l} |\boldsymbol{o}_e(k,l) - \boldsymbol{o}(k,l)|^2$. Thanks to Parseval's

theorem, this error can also be written:

$$\epsilon^2 = \iint |\tilde{o}_e - \tilde{o}|^2(\nu_x, \nu_y) d\nu_x \, d\nu_y. \tag{3}$$

For the design of an operational system, there exists a frequency domain of interest $\mathcal{D}$ given by the resolution needed for the considered mission. For simplicity we consider that this domain is a disk of radius $\nu_{\text{max}} = B/\lambda$, called the maximum frequency of interest. As a consequence, the metric of interest is rather:

$$\epsilon^2_{\mathcal{D}} = \iint_{(\nu_x,\nu_y)\in\mathcal{D}} |\tilde{o}_e - \tilde{o}|^2(\nu_x, \nu_y) d\nu_x \, d\nu_y. \tag{4}$$

The approach we take is that of experiment planning: the optimal aperture configuration is the one that yields the smallest error, on average for a class of objects and a large number of noise outcomes. Let $\varepsilon_{\mathcal{D}}$ be this average error, plugging Eqs. (1) and (2) into Eq. (4) and averaging the latter yields:

$$\begin{aligned} \varepsilon^2_{\mathcal{D}} &\triangleq \langle \epsilon^2_{\mathcal{D}} \rangle_{\boldsymbol{o},\boldsymbol{n}} \\ &= \iint_{(\nu_x,\nu_y)\in\mathcal{D}} \frac{S_n(\nu_x, \nu_y) \, d\nu_x \, d\nu_y}{|\tilde{h}|^2(\nu_x, \nu_y) + S_n/S_o(\nu_x, \nu_y)} \end{aligned} \tag{5}$$

For a white noise, this simplifies further:

$$\varepsilon^2_{\mathcal{D}} \propto \iint_{(\nu_x,\nu_y)\in\mathcal{D}} \frac{d\nu_x \, d\nu_y}{|\tilde{h}|^2(\nu_x, \nu_y) + S_n/S_o(\nu_x, \nu_y)}. \tag{6}$$

This result extends earlier work based on the same approach[27] in that it uses a Wiener filter instead of an inverse filter truncated to the maximum frequency of interest ν_{max}. In particular, if we consider that the SNR is high below this frequency ($S_n/S_o \to 0$) then Eq. (6) reduces to

$$\varepsilon^2_{\mathcal{D}} \propto \iint_{(\nu_x,\nu_y)\in\mathcal{D}} \frac{1}{|\tilde{h}|^2(\nu_x, \nu_y)} \, d\nu_x \, d\nu_y, \tag{7}$$

which is equivalent to Eq (19) of [27].

The numerical minimization of Eq. (6) with respect to the positions of the individual telescopes has been implemented by means of a conjugate-gradient method and yields the optimal configurations, for a given number of sub-apertures of a given size.

Note that this approach can be extended [28] to an instrument that is rotating, so as to synthesize an aperture in time. This is a natural and effective way to reduce the size and number of the sub-apertures, as noted by Guyon[29].

4.3 Simulations

In the simulations presented here we consider that S_n/S_o is a constant equal to 10^{-4}, which corresponds for instance to recording a point-source with a total flux of 10^4 photons and a negligible detector noise. The minimization of the metric defined in Eq. (6) has been performed numerically for various numbers of sub-apertures and various diameters for each sub-aperture, in order to yield the optimal configuration. In practice, because we currently use a gradient-based minimization and the metric has several local minima, it is necessary to use several starting points to get to the global

minimum. At this minimum, the value of the metric is very informative, as it gives the average error on the restored object. The diameter of the sub-apertures can be increased until this error is considered reasonable.

Figure 7 shows the configuration optimized in snapshot mode for 9 and 12 sub-apertures. For 12 sub-apertures, the diameter is about 20% smaller than for 9. Complementary simulations show that for a rotating instrument, 7 sub-apertures are enough to obtain a good frequency coverage, even with a diameter 50% smaller than for 9 sub-apertures in snapshot mode.

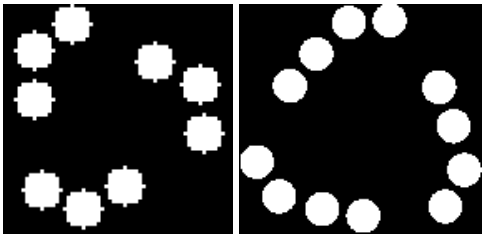

Figure 7: Optimal aperture configurations obtained with 9 (left) and 12 telescopes (right).

5 Image restoration

We have developed a data processing method suited to a MAOT. It differs from methods of image reconstruction from interferometric data used in astronomy[30] because a MAOT records a continuous set of the observed object's spatial frequencies and not a discrete one. The appropriate processing is an image restoration, whose aim is to compensate for the intrinsically low Modulation Transfer Function of such an instrument (see Fig. 8) while preserving the informative elements in the image such as edges, which are present in all man-made constructions. This restoration method is adapted

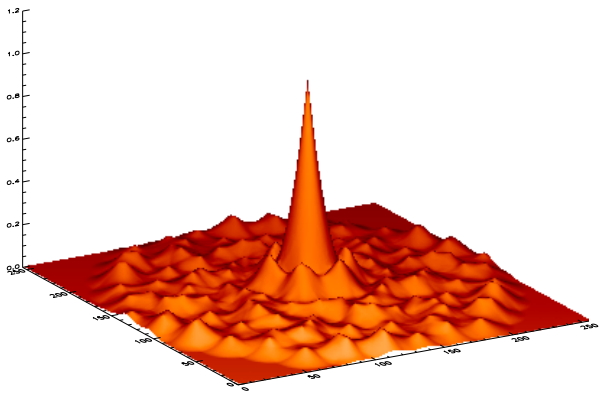

Figure 8: Modulation Transfer Function of the 12-telescope aperture configuration shown on the right part of Fig. 7.

from developments performed for Space observation and can cope with an imperfect knowledge of the transfer function of the instrument [31]. Figure 9 shows the simulation of the complete instrumental chain, *i.e.*, acquisition and restoration. The comparison between the image that would be obtained with a single aperture (Fig. 9b) and the one obtained with the complete instrument (Fig. 9c) simultaneously shows the presence of high spatial frequency information in the latter image and the attenuation of these high frequencies by the instrument. These images take into account the optical and the detector transfer functions and have a noise level corresponding to an average of 30000 photo-electrons per pixel. Figure 9d shows that the proposed method leads to a restored object that is very close to the original one (Fig. 9a): it restores the sharp edges of the object and simultaneously avoids noise amplification.

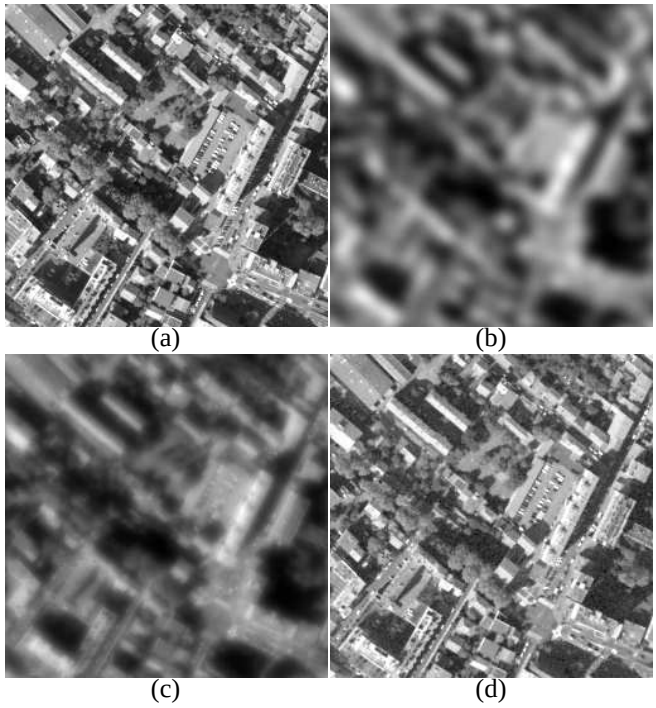

Figure 9: Observed object (a), image seen by a single aperture (b), image recorded by the complete MAOT (c) and restored image (d).

6 Acknowledgments

We are grateful to V. Bentadj, C. Coudrain, B. Fleury, F. Mendez, J. Montri and L. Rousset-Rouvière for making the BRISE experimental testbed happen. We thank D. Laubier (CNES) for making an independent confirmation of section 2 by computing our design performance with the Zemax software and for providing Fig. 2. Lastly, we acknowledge DGA/SPOTI for the financial support of part of this study.

7 Conclusion

Together, these results show that the permanent and high-resolution monitoring of our planet is a breakthrough that is possible with current technology, and could constitute a challenging yet federating and enthusing project.

References

[1] G. Rousset, L. M. Mugnier, F. Cassaing, and B. Sorrente. Imaging with multi-aperture optical telescopes and an application. *C. R. Acad. Sci. Paris*, Série IV, tome 2(1):17–25, January 2001.

[2] W. A. Traub. Combining beams from separated telescopes. *Appl. Opt.*, 25(4):528–532, February 1986.

[3] D. W. Mac Carthy, P. A. Strittmatter, E. K. Hege, and F. J. Low. Performance of the multiple mirror telescope (MMT) VIII. MMT as an optical-infrared interferometer and phased array. In *Advanced technology optical telescopes*, volume 332, pages 57–64. Proc. Soc. Photo-Opt. Instrum. Eng., 1982.

[4] C. R. De Hainaut, D. C. Duneman, R. C. Dymale, J. P. Blea, B. D. O'Neil, and C. Hines. Wide field performance of a phased array telescope. *Opt. Eng.*, 34(3):876, March 1995.

[5] V. Zarifis et al. The Multi Aperture Imaging Array. In S. Unwin and R. Stachnik, editors, *Working on the Fringe: optical and IR interferometry from ground and space*, volume 194 of *Astron. Soc. Pacific Conf. Series*, pages 278–285, Dana Point, May 1999.

[6] T. W. Stuhlinger. All-reflective phased array imaging telescopes. In *International lens design conference*, volume 1354, pages 438–446. Proc. Soc. Photo-Opt. Instrum. Eng., 1990.

[7] L. M. Mugnier, F. Cassaing, G. Rousset, and B. Sorrente. Earth observation from a high orbit: pushing the limits with synthetic aperture optics. In *Space-based observation techniques*, Samos, Greece, October 2000. NATO/RTO-SET.

[8] L. D. Weaver, J. S. Fender, and C. R. De Hainaut. Design considerations for multiple telescope imaging arrays. *Opt. Eng.*, 27(9):730–735, September 1988.

[9] J. E. Harvey and C. Ftaclas. Field-of-view limitations of phased telescope arrays. *Appl. Opt.*, 34(25):5787–5798, September 1995.

[10] F. Cassaing. *Analyse d'un instrument à synthèse d'ouverture optique : méthodes de cophasage et imagerie à haute résolution angulaire*. PhD thesis, Université Paris XI Orsay, December 1997.

[11] R. L. Lucke. Influence of Seidel distortion on combining beams from a phased telescope array. *Appl. Opt.*, 38(22):4776–4783, August 1999.

[12] F. Cassaing, B. Sorrente, B. Fleury, and D. Laubier. Optical design of a Michelson wide-field multi-aperture telescope. In *Optical System Design*, volume 5249, Saint-Etienne, France, 2003. Proc. Soc. Photo-Opt. Instrum. Eng.

[13] F. Cassaing, L. Mugnier, G. Rousset, and B. Sorrente. Éléments-clés de la conception d'un instrument spatial à synthèse d'ouverture optique. In *International Conference on Space Optics*, Toulouse (France), December 1997. CNES.

[14] M.-T. Velluet, V. Michau, and G. Rousset. Wavefront sensors for the active control of earth observation optical instruments. In *International Conference on Space Optics*, Toulouse (France), December 1997. CNES.

[15] M. Shao, M. M. Colavita, B. E. Hines, D. H. Staelin, D. J. Hutter, K. J. Johnston, D. Mozurkewich, R. S. Simon, J. L. Hershey, J. A. Hughes, and G. H. Kaplan. The Mark III Stellar Interferometer. *Astron. Astrophys.*, 193:357–371, March 1988.

[16] B. Sorrente, F. Cassaing, G. Rousset, S. Robbe-Dubois, and Y. Rabbia. Real-time optical path difference compensation at the Plateau de Calern I2T interferometer. *Astron. Astrophys.*, 365:301–313, 2001.

[17] L. Damé. http://must.aerov.jussieu.fr/.

[18] B. Sorrente, F. Cassaing, F. Baron, C. Coudrain, B. Fleury, F. Mendez, V. Michau, L. Mugnier, G. Rousset, L. Rousset-Rouvière, and M.-T. Velluet. Multiple-aperture optical telescopes: cophasing sensor testbed. In *5th International Conference On Space Optics*, volume SP-554, pages 479–484, Toulouse, France, 2004. CNES/ESA, ESA.

[19] R. A. Gonsalves. Phase retrieval and diversity in adaptive optics. *Opt. Eng.*, 21(5):829–832, 1982.

[20] R. G. Paxman and J. R. Fienup. Optical misalignment sensing and image reconstruction using phase diversity. *J. Opt. Soc. Am. A*, 5(6):914–923, 1988.

[21] J. H. Seldin, R. G. Paxman, V. G. Zarifis, L. Benson, and R. E. Stone. Closed-loop wavefront sensing for a sparse-aperture, phased-array telescope using broadband phase diversity. In *Imaging technology and telescopes*, volume 4091 of *Proc. Soc. Photo-Opt. Instrum. Eng.*, July 2000.

[22] A. Blanc. *Identification de réponse impulsionnelle et restauration d'images : apports de la diversité de phase*. PhD thesis, Université Paris XI Orsay, July 2002.

[23] A. Blanc, L. M. Mugnier, and J. Idier. Marginal estimation of aberrations and image restoration by use of phase diversity. *J. Opt. Soc. Am. A*, 20(6):1035–1045, 2003.

[24] F. Baron, F. Cassaing, A. Blanc, and D. Laubier. Cophasing a wide field multiple-aperture array by phase-diversity: influence of aperture redundancy and dilution. In M. Shao, editor, *Interferometry in Space*, volume 4852, Hawaii, USA, 2002. Proc. Soc. Photo-Opt. Instrum. Eng., SPIE.

[25] A. Schumacher, N. Devaney, and L. Montoya. Phasing segmented mirrors: a modification of the keck narrow-band technique and its application to extremely large telescopes. *Appl. Opt.*, 41(7):1297–1307, March 2002.

[26] F. Baron. *Définition et test d'un capteur de cophasage sur télescope multipupilles: application à la détection d'exoplanètes et à l'observation de la Terre*. PhD thesis, Ecole Doctorale d'Astronomie et d'Astrophysique d'Ile de France, 2005.

[27] L. M. Mugnier, G. Rousset, and F. Cassaing. Aperture configuration optimality criterion for phased arrays of optical telescopes. *J. Opt. Soc. Am. A*, 13(12):2367–2374, December 1996.

[28] L. Mugnier, F. Cassaing, B. Sorrente, F. Baron, M.-T. Velluet, V. Michau, and G. Rousset. Multiple-aperture optical telescopes: some key issues for Earth observation from a GEO orbit. In *5th International Conference On Space Optics*, volume SP-554, pages 181–187, Toulouse, France, 2004. CNES/ESA, ESA.

[29] O. Guyon and F. Roddier. Aperture rotation synthesis: optimization of the (u, v)-plane coverage for a rotating phased array of telescopes. *Pub. Astron. Soc. Pacific*, 113:98–104, January 2001.

[30] S. Meimon, L. M. Mugnier, and Guy Le Besnerais. A convex approximation of the likelihood in optical interferometry. *J. Opt. Soc. Am. A*, accepted.

[31] L. M. Mugnier, T. Fusco, and J.-M. Conan. MISTRAL: a myopic edge-preserving image restoration method, with application to astronomical adaptive-optics-corrected long-exposure images. *J. Opt. Soc. Am. A*, 21(10):1841–1854, October 2004.